Open Access

Advances in Environmental and Engineering Research

LIDSEN Publishing Inc.

Original Research

The Dynamics of the Oceanic Air-Sea Boundary Layer

John A. T. Bye *

School of Geography, Earth and Atmospheric Sciences, The University of Melbourne, Victoria 3010, Australia; E-Mail: jbye@unimelb.edu.au

* **Correspondence:** John A. T. Bye; E-Mail: jbye@unimelb.edu.au

Academic Editor: Shih-Ang (S. A.) Hsu

Special Issue: Air-Sea Interaction and Marine Meteorology

Adv Environ Eng Res
2023, volume 4, issue 1
doi:10.21926/aeer.2301018

Received: November 13, 2022
Accepted: January 25, 2023
Published: February 05, 2023

Abstract

This paper presents a model for the similarity structure of the velocity profiles in air and water in the wave boundary layer, which provides predictions in terms of two parameters, F and R, of all its important properties, including the Charnock parameter, the surface drift velocity and the condition for the cancellation of the surface Stokes velocity by the surface current. The parameter, F, arises from the fetch variability of the wave field, and the parameter, R, arises from the duration variability of the wave field. In the analysis two regimes emerge, namely the Ekman regime and the Hasselmann regime. In the Ekman regime, which occurs for $R > \frac{1}{2}(1 + F)$, there is a net loss of energy from the wave field to the deep ocean, and in the Hasselmann regime which occurs for $R < \frac{1}{2}(1 + F)$, there is a net gain of energy from the atmosphere to the wave field. The predictions are compared with observations from classical wave formulae, wind-wave studies, and also ROMS and SWAN modelling in the South Australian Basin. A general conclusion is that the condition, $F = 1$, which was used in the original inertial coupling model of Bye [1], is a good approximation for large scale theoretical ocean studies, and hence the wind-wave interaction is determined principally by R.

Keywords

Air-sea interaction; similarity air and water velocity profiles in the wave boundary layer; the Charnock parameter; the inertial coupling relation; classical wave prediction formulae; wind-wave campaign data; regional ocean modelling system and simulating waves nearshore modelling results; energy supply to the deep ocean by the wave spectrum

1. Introduction

The importance of wind–wave research from an Australian perspective has been recently highlighted in Greenslade [2] where several aspects of this important topic were discussed, however a background theoretical study of air-sea research in the wave boundary layer was not included in this work.

Here, a background paper is given in which theoretical results on air-sea interaction, based on a similarity model, are presented (Section 2) and compared with various observational studies, both recent and historical (Section 3) with which it is suggested that there is general agreement.

The main feature of this model of the oceanic air-sea boundary layer is that it treats both fluids which occur in the wave boundary layer as a coupled system. In Section 2.1, the similarity relations for the velocity profiles in the air and water are presented, and it is pointed out that in the air the profile arises from aerodynamically rough flow, whereas in the water the profile arises from irrotational wave motions. Section 2.2 makes a clear distinction between the Lagrangian and Eulerian velocity in the water, and Section 2.3 introduces the Ekman and Hasselmann regimes which control the energy transfers from and to the wave field, through two parameters (R and F) which arise respectively from the duration and fetch of the meteorological forcing. Section 2.4 provides an expression for the Charnock parameter in terms of R and F. The surface Stokes velocity is derived in Section 2.5, and the relation between the surface current and the surface Stokes velocity is considered in Section 2.6, which indicates how cancellation of the surface Stokes velocity occurs. Finally, the surface drift velocity in terms of R and F is obtained in Section 2.7. The model thus provides connected theoretical predictions for all the important properties of the air-sea, wind-wave boundary layer.

Section 3 summarizes the observational data, including the classical wave formulae (Section 3.1), wind-wave data (Sections 3.2 and 3.3), and the results from ROMS and SWAN regional modelling (Section 3.4) which are all compared with the predictions of Section 2.

Section 4 concludes that the substitution of F = 1 in the similarity relations, which was used in the original inertial coupling model, is appropriate for large scale ocean modelling studies, and in Section 4.1 the application of the F = 1 model in two reference frames is considered. Section 5 is a brief Conclusion.

2. The Air-Sea Boundary Layer Model

2.1 The Similarity Profile Relations for Air and Water

The longitudinal components of the similarity relations for air and water, presented in Bye and Wolff [3] are,

$$u_{Ro}(z) - u_o = Fu_L + u_*/\kappa \ln(z/z_R), z_R \le z \le z_B \quad (1a)$$

$$u_{St}(-z) - u_o = \varepsilon u_L - w_*/\kappa \ln(z/z_R), z_R \le z \le z_B \quad (1b)$$

in which it is assumed that the surface shear stress lies along ox ($\underline{\tau}_s = \tau_s, 0$), $\tau_s > 0$ where $\tau_s = \rho_1 u_*^2 = \rho_2 w_*^2$ in which u_* and w_* are respectively the frictional velocities in air and water, and ρ_1 and ρ_2 are respectively the densities of air and water, and oz is vertically upwards in which z = 0 is the mean air-water interface. $u_{Ro}(z)$ denotes aerodynamically rough flow in the air, and $u_{St}(-z)$ denotes the Stokes velocity in the water, which has been expressed in terms of a wall boundary layer [4] derived from the truncated Toba spectrum [5].

$$\phi(\sigma) = \beta u_* g \sigma^{-4}, \sigma_0 \le \sigma \le \sigma_1 \quad (2)$$

in which g is the acceleration of gravity and β is a constant, and the frequency, $\sigma = (gk)^{1/2}$ where k is the wavenumber, and in (1a) and (1b), $z_R = 1/(2k_1)$ and $z_B = 1/(2k_o)$ are respectively the high and low wavenumber cut-offs of the spectrum, and κ is von Karman's constant, $\varepsilon = (\rho_1/\rho_2)^{1/2}$, and u_o is a reference velocity, which is zero in the Earth's reference frame. $\varepsilon u_L = u_{St}(-z_R) - u_o$ is the wave induced velocity in the water (the surface Stokes velocity) and $Fu_L = u_{Ro}(z_R) - u_o$ is the wave induced velocity in the air (the spectrally weighted phase velocity). Hence, the ratio of the wave induced velocity in the air to that in the water is F/ε.

At the edge of the wave boundary layer ($z = \pm z_B$), $u_{Ro}(z_B) = u_1$ and $u_{St}(-z_B) = u_2$ in which u_1 and u_2 are respectively the surface wind and the surface current which are determined by thermohaline processes outside of the wave boundary layer ($z_B \ge z \ge -z_B$). For the Toba spectrum (2), since $u_{St}(-z_B) - u_o = 0$,

$$\varepsilon u_L = \varepsilon u_L)_{To} \quad (3)$$

where $\varepsilon u_L)_{To} = w_*/\kappa \ln(z_B/z_R)$, >0.

On eliminating u_L between 1(a) and 1(b), the relation,

$$(u_1 - u_o) - F/\varepsilon(u_2 - u_o) = (1 + F)u_*/\kappa \ln z_B/z_R \quad (4)$$

is obtained, which on rearranging yields the drag relation,

$$u_* = K_F{}^{1/2}\left(u_1 - u_o - F/\varepsilon(u_2 - u_o)\right) \quad (5)$$

where $K_F = ((1 + F)/\kappa \ln z_B/z_R)^{-2}$, and the ratio of the surface wind to the surface current (F/ε) is the same as that for the wave induced velocities in the two fluids, and for F = 1, K_F reduces to the inertial drag coefficient,

$$K_I = (2/\kappa \ln z_B/z_R)^{-2} \quad (6)$$

[1, 6].

On substituting (6) in (3), the wave induced velocity due to the truncated Toba spectrum,

$$\varepsilon u_L)_{To} = 1/2 w_*/K_I{}^{1/2} \quad (7)$$

or, alternatively, on eliminating the logarithmic term between (1a) and (1b), yields the relation,

$$\varepsilon u_L = [\varepsilon(u_1 - u_o) + (u_2 - u_o)]/(1 + F) \tag{8}$$

2.2 The Lagrangian and Eulerian Shears in the Water

On substituting for $(u_2 - u_o)$ in (8) from the relation,

$$\varepsilon u_L + r(u_2 - u_o) = 0 \tag{9}$$

which was introduced in Bye and Wolff [6] to relate the Lagrangian shear (εu_L) and the Eulerian shear $(u_2 - u_o)$ in the oceanic boundary layer, we obtain, $u_1 - u_o = u_L(1 + F + 1/r)$, and from (1a) evaluated at $z = z_B$, using (7), $u_1 - u_o = Fu_L + \frac{1}{2}u_*/K_I^{1/2}$, from which, on eliminating u_L, it is found that,

$$u_* = K_I^{1/2}(u_1 - u_o)/R \tag{10}$$

where

$$R = 1/2\big(1 + Fr/(1 + r)\big) \tag{11a}$$

and

$$r = (2R - 1)/(1 + F - 2R) \tag{11b}$$

Alternatively on substituting for $(u_1 - u_o)$ in (10) yields,

$$\varepsilon u_L/w_* = 1/2(2R - 1)/\big(FK_I^{1/2}\big) \tag{12}$$

Eq. (10) enables R to be evaluated in terms of observable quantities. Thus, on making use of the logarithmic velocity profile in the air (10), may be expanded to yield, $(u_{10} - u_o) + (u_1 - u_{10}) = Ru_*/K_I^{1/2}$, which yields the relation,

$$R = K_I^{1/2}\big(K_{10}^{-1/2} + \kappa^{-1}\ln(z_B/10)\big) \tag{13}$$

where $z_B = gT^2/8\pi^2$ in which $T = 2\pi/(gk_o)^{1/2}$ is the peak wave period. Eq. (13) is identical with the expression for R for F = 1 in Bye and Wolff [7], and is shown in Figure 1. The important feature of Figure 1 is that R increases with T at a constant u_*. This occurs as the duration of the wind forcing increases and swell is developed.

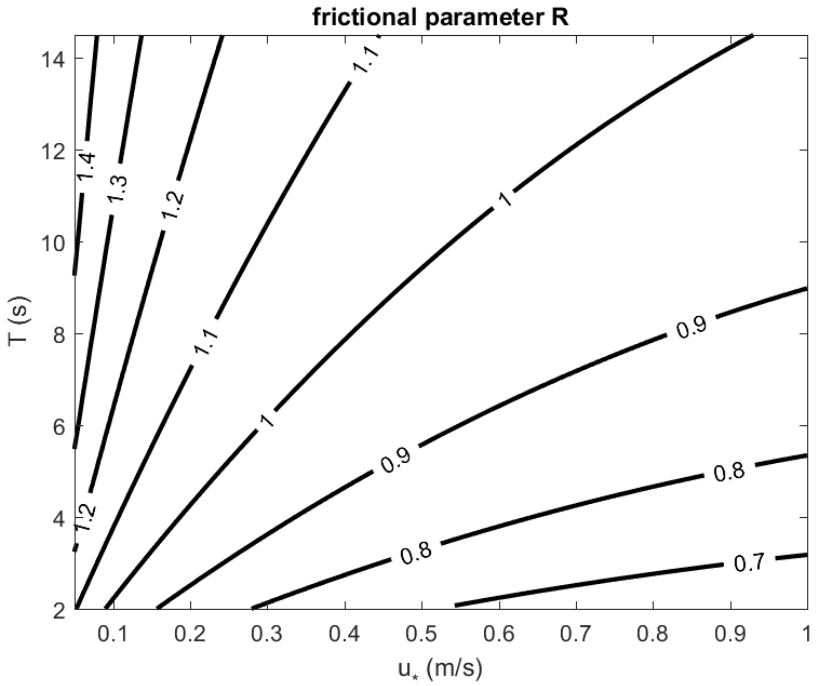

Figure 1 The parameter (R) as a function of u_* and T evaluated from equation (A1) in the Appendix of Bye et al. [8] with K_{10m} = 0.002 and u_{10m} = 40 ms^{-1} and reproduced from Figure 2 of Bye et al. [7].

On substituting for εu_L from (12) in (9) using (11b), It is also found that,

$$u_2 - u_o = w_*\big(R - 1/2(1+F)\big)/\big(F{K_I}^{1/2}\big) \tag{14}$$

2.3 Ekman and Hasselmann Regimes

Eq. (14) is of high significance as for $R > R_c$ where,

$$R_c = 1/2(1+F) \tag{15}$$

$u_2 - u_o$ has the same sign as w_*, and hence the surface current can support an Ekman regime, whereas for $R < R_c$ $u_2 - u_o$ opposes the surface shear stress and an Ekman regime is not supported and instead a Hasselmann regime occurs. We use these names to emphasize the physical difference between the two regimes. In the Ekman regime there is a net loss of energy from the wave field to the deep ocean, whereas in the Hasselmann regime there is a net gain of energy from the atmosphere to the wave field. There is no net transfer of energy to or from the wave field for $R = R_c$, which is the condition for the fully developed sea. For F = 1, R_c = 1.

On now turning to the evaluation of the wave induced velocity in the air, the spectrally weighted phase velocity of the gravity waves due to the truncated Toba spectrum is,

$$Fu_L)_{To} = g/\sigma_M \tag{16}$$

where $\sigma_M^2 = \int^{\sigma}{}_1,^{\sigma}{}_o \sigma^2 \phi(\sigma) d\sigma / \int^{\sigma}{}_1,^{\sigma}{}_o \phi(\sigma) d\sigma$, from which,

$$Fu_L)_{To} = c_o\big[\big(1 + k_o/k_1 + (k_o/k_1)^{1/2}\big)/3\big]^{1/2} \tag{17}$$

in which c_o is the phase speed of the peak wave [3], and since $c_o > 0$, $F > 0$. On expressing the cut-off wavenumber ratio (k_o/k_1) in terms of the inertial drag coefficient (K_I) from (6), $k_o/k_1 = \exp(-½\kappa K_I^{-1/2})$, and hence on substituting for k_o/k_1 in (17) with $\kappa = 0.40$ and $K_I = 0.0015$ [6], it is found that,

$$\mathrm{Fu_L})_{To} = 0.60c_o \tag{18}$$

which, on substituting for $u_L)_{To}$ from (7), yields the expression for the wave age,

$$c_o/u_* = 21.5F \tag{19}$$

where $1/(1.20K_I^{1/2}) = 21.5$.

2.4 The Charnock Parameter

Eq. (19) can be used to obtain a prediction for the Charnock parameter (α), defined by the relation, $z_o = \alpha u^{*2}/g$, in which z_o is defined relative to the reference velocity, u_o [9]. Using the logarithmic identity $\ln z_o/z_B = \ln z_R/z_B + \ln z_o/z_R$, in which from (6), the first term, $\ln z_R/z_B = -½\kappa/K_I^{1/2}$, and from (1a) evaluated at $u = u_o$, on substituting for εu_L from (12), the second term, $\ln z_o/z_R = -½(2R - 1)\kappa/K_I^{1/2}$. Hence, $z_o/z_B = \exp(-\kappa R K_I^{-1/2})$, which on expressing z_B in terms of the wave speed of the peak wave (c_o) yields,

$$\alpha = 1/2(c_o/u_*)^2\exp\left(-\kappa R K_I^{-1/2}\right) \tag{20}$$

Eq. (20) is an expression for the Charnock parameter [9] which for R = 1 depends only on the inertial drag coefficient and the wave age [6], or alternatively, on substituting (19) in (20),

$$\alpha = 1/2(21.5F)^2\exp\left(-\kappa R K_I^{-1/2}\right) \tag{21}$$

Eq. (19) is a direct prediction for c_o/u_* in terms of F, and (21) is a prediction for α in terms of the two parameters (F and R) which arise respectively from the fetch variability and the duration variability of the wave field.

2.5 The Surface Stokes Velocity

On evaluating the ratio of the wave induced velocity due to the truncated Toba spectrum $(\varepsilon u_L)_{To}$ from (7) to the wave induced velocity (εu_L) from (12), the ratio,

$$\varepsilon u_L)_{To}/\varepsilon u_L = F/(2R - 1) \tag{22}$$

and hence, on substituting for F from (15), it is found that,

$$\varepsilon u_L)_{To}/\varepsilon u_L = (2R_c - 1)/(2R - 1) \tag{23}$$

which indicates that the Toba truncated spectral model, $\varepsilon u_L)_{To}$, underestimates the wave induced velocity (εu_L) in the Ekman regime and overestimates it in the Hasselmann regime, It is suggested that the physical processes which gives rise to this response are that in the Ekman regime, the transfer of energy from the wave field to the deep ocean occurs through the promotion of long

period waves which, as pointed out in Bye and James [10], would lead to a low wavenumber tail, which is absent in the truncated Toba spectral model. Conversely, in the Hasselmann regime, the transfer of energy from the atmosphere to the wave field is promoted by long period waves which are over estimated by the truncated Toba spectral model.

2.6 The Relation between the Surface Stokes Velocity and the Surface Current

The sum of the surface Stokes velocity and the surface current, relative to the reference velocity, $\varepsilon u_L + (u_2 - u_o)$, can be expressed solely in terms of εu_L using (9) and (11b) which yields,

$$\varepsilon u_L + (u_2 - u_o) = (4R - 2 - F)/(2R - 1)\varepsilon u_L \tag{24}$$

Hence the sum of the wave induced and turbulent velocities ($\varepsilon u_L + u_2 - u_o$) is zero for $R = R_{can}$, where,

$$R_{can} = 1/4(F + 2) \tag{25a}$$

such that for F = 1, the surface current cancels the surface Stokes velocity when R = ¾ and also the ratio,

$$R_{can}/R_c = (1 + 1/2F)/(1 + F) \tag{25b}$$

Hence from (25b) the cancellation always occurs in the Hasselmann regime, and at low fetches ($F \rightarrow 0$), since $R_{can}/R_c \rightarrow 1$, it can occur with no net energy transfer to or from the wave field as postulated in [11].

More generally, from (24), the ratio of the Eulerian and Lagrangian shears,

$$(u_2 - u_o)/\varepsilon u_L = 1 - (2R_c - 1)/(2R - 1) \tag{26a}$$

$$= 1 - F/(2R - 1) \tag{26b}$$

which is a measure of the titanic struggle of Euler and Lagrange in determining the current outcome, that is occurring as F and R vary. The ratio of the Eulerian and Lagrangian shears is negative in the Hasselmann regime, positive in the Ekman regime and zero in the fully developed sea.

The increase in the relative importance of $(u_2 - u_o)$ in the Ekman regime as R increases is of particular significance as this wave-current interaction increases the transfer of energy from the wave field to the deep ocean. This important process does not appear to have been highlighted previously in advanced wave modelling studies, e.g. Babanin et al [12].

2.7 The Surface Drift Velocity

The matching of the air and water velocities occurs through the drift velocity.

On assuming that the velocities in the two fluids are continuous across the interface, and equating the velocities in 1(a) and 1(b), we obtain, $u_*/\kappa \ln z_s/z_R = (\varepsilon - F)u_L/(1 + \varepsilon)$ in which z_s is the roughness length at the edge of the drift layer, from which,

$$u_s - u_o = (1 + F)\varepsilon u_L/(1 + \varepsilon) \tag{27}$$

where (u_s - u_o) is the drift velocity, which on using (12) may also be expressed as,

$$u_s - u_o = 1/2(2R - 1)(1 + F)/\left(FK_i^{1/2}\right)w_*/(1 + \varepsilon) \tag{28}$$

For F = 1, from (27), the ratio of the surface drift velocity to the surface Stokes velocity, relative to the reference velocity,

$$(u_s - u_o)/\varepsilon u_L = 2/(1 + \varepsilon) \tag{29}$$

3. Observations

There are several types of observations with which the results of the model can be compared. These observational results are considered below. Special emphasis will be placed on, under which conditions, F = 1, which was proposed in the original inertial coupling analysis [1], is a good approximation.

3.1 Classical Wave Formulae

In the early wave models, the peak wave period (T) was predicted in terms of the 10 m wind speed (u_{10}) and also the fetch and duration. These models lead to a dimensional expression of the form,

$$T = A_o u_{10}/g \tag{30}$$

where g is the acceleration of gravity and A_o is an observationally determined constant, which may depend on fetch and duration, and asymptotes to a limiting value at large fetches and durations. On expressing (30) in terms of the friction velocity in air ($u_* = (\tau_s/\rho_1)^{1/2}$) where τ_s is the surface shear stress and ρ_1 is the air density, we obtain,

$$c_o/u_* = a_o \tag{31}$$

in which $a_o = A_o/(2\pi K_{10}^{1/2})$, where K_{10} is the 10 m drag coefficient. Eq. (31) has the form of the wave age (19).

In a coastal sea, observations for the fully developed sea indicate that A_o = 8.6 [13] from which, using a 10 m drag coefficient, K_{10} = 0.002, we obtain, a_o = 30.6, and hence on substituting for c_o/u_* from (31), at large fetches, F = F_{max} where F_{max} = 1.42. Thus the similarity model (1a and b) would apply over the range of surface parameter ($0 \le F \le F_{max}$) in which at small fetches $F \to 0$. Fetch dependent observations also indicate that the peak period (T) is proportional to $x^{1/3}$ where x is the fetch [14], hence the mean peak period over the fetch length is ¾ T from which it follows that the predicted value for the mean conditions is F is 1.07, which is very similar to the condition, F = 1.

In summary, the model, with F = 1, applies for the mean values of u_* and c_o which occur over the fetch length (x).

3.2 Wind-wave Studies

As was seen in Section 3.1, the variability of F in the coastal sea can be attributed to a fetch dependence of the fully developed wave field. A similar variability would occur in more general wave conditions. This variability has been observed in wind-wave studies, and is conveniently documented in Figure 1 of Bye et al. [15], which is reproduced from Figure 12 of Donelan et al [16] on to which contours of R using (13) have been added. The data points from the various wind-wave studies are shown as a function of inverse wave age (u_*/c_o) and R. For each data point, F can be determined from (19) and hence R_c from (15).

The main group of observational points, which excludes the HEXOS, wave tank and Lake Ontario data groups, has the approximate parameter values of R ≈ 0.95 and c_o/u_* ≈ 20, which yield F ≈ 0.93 and R_c ≈ 0.97.

The parameters for the cluster of points from the HEXOS data set are R ≈ 0.75 and c_o/u_* ≈ 11.8. Hence F ≈ 0.55 and R_c ≈ 0.78, and the Lake Ontario group, has the approximate parameter values of R ≈ 0.6 and c_o/u_* ≈ 5, from which F ≈ 0.23 and R_c ≈ 0.62.

Hence $R < R_c$ for the three data groups, which indicates that in the wind-wave studies, a Hasselmann regime occurred. This was biased towards the low end of wave development at the fetches prevailing in all three data groups in which F < 1, in particular for the HEXOS and Lake Ontario data sets (F << 1).

3.3 The Cancellation of the Surface Drift by the Surface Current

In the Lake Ontario group of the wind-wave observations in Section 3.2, F ≈ 0.23, and R ≈ 0.6, which is similar to the theoretical prediction for cancellation (25a) of R_{can} ≈ 0.56, i.e. close to the cancellation condition, and is also similar to R_c ≈ 0.62. Thus here we have a regime in which there is almost no net energy transfer to or from the wave field and also cancellation of the surface drift by the surface current is occurring, as shown in Section 2.6 for $F \rightarrow 0$ This is an exceedingly interesting and unusual observational situation, which closely mirrors the prediction for cancellation proposed by Hasselmann [11] which is discussed in Section 2.6.

3.4 Wave Transport in the South Australian Basin

In a recent wind-wave study [10] for the South Australian Basin during the period 2010-2012 the wave environment was dominated by swell, generated in the storm systems, with a monthly average peak wave period (T) of about 11 s (c_o = 17 ms^{-1}, z_B = 15 m), and the median values obtained from histograms of R over daily averages from the Regional Ocean Modelling System (ROMS) using (15) was R = 1.19, and from the Simulating Waves Nearshore (SWAN) using (16) with F = 1 to evaluate u_2 and $v_2 = -u_2$, was R = 1.17. The similar magnitudes of these two independent estimates of R strongly supports the existence of an Ekman regime in which F = 1.

The daily (i) SWAN spectral transport $U_{sw}(i) = \int^{\infty,o}\sigma\phi_i(\sigma)d\sigma)$ and the Toba spectral transport ($U_{To}(i) = z_B w_*/\kappa)_i$) were also evaluated over the two year period, 2011–2012 [10]. Figure 2 shows that at low values there is a cluster of data points in which $U_{sw}(i)$ and $U_{To}(i)$ are approximately equal and hence from (23), since F = 1, R = 1 as found for the mean wave conditions in the classical wave studies (Section 3.1), At higher values, however, there is a pronounced linear trend in which $U_{sw}(i) = 1.36U_{To}(i)$ as predicted by (22) for the observed median parameter, R = 1.18 and F = 1. The

regression slope of best fit (1.16) is a split between the data points of the two physical models. It is concluded, on the assumption that the transports are proportional to the wave induced velocity in the water (εu_L), that the cluster of low value points in Figure 2 is due to the fully developed coastal circulation in which R = 1 (Section 3.1) and more importantly that the trend in the higher value points is consistent with open ocean conditions in which the predicted ratio (23) is applicable.

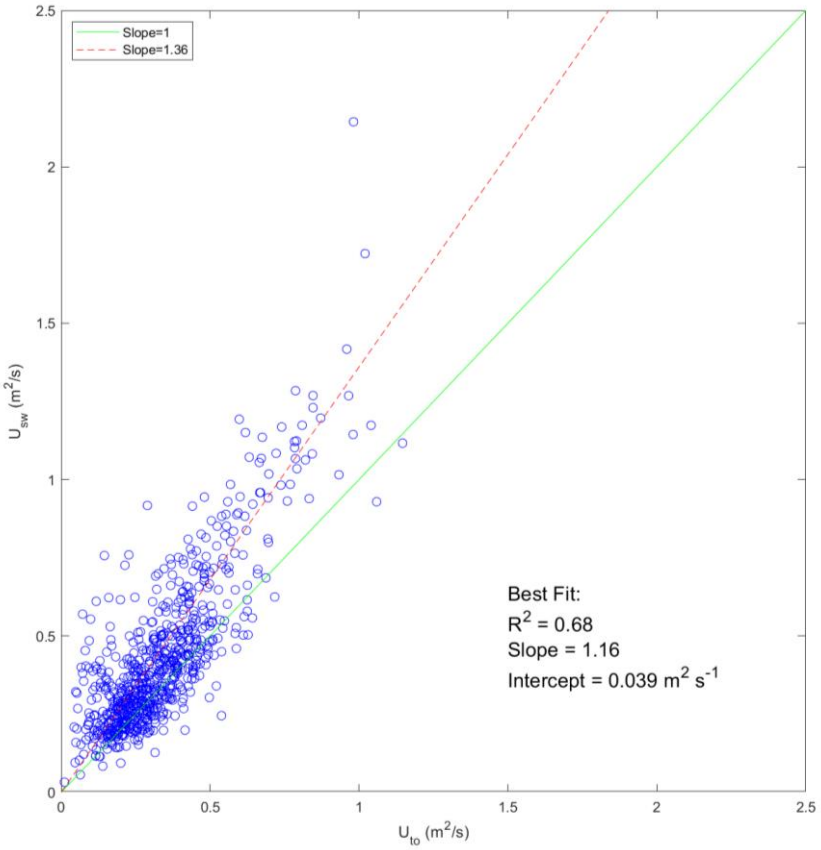

Figure 2 The linear regression of the daily SWAN spectral transport and the daily truncated Toba spectral transport for the period 2011-2012 in the South Australian Basin reproduced from Figure 9 of Bye and James [10], with the inclusion of the linear relation (22).

3.5 The Fully Developed Sea

The concept of the fully developed sea is well known, see for example, Jones and Toba [17]. In the model, from (15), the fully developed sea occurs for R = ½(1 + F), from which the wave age (c_o/u_*) and the Charnock parameter (α) in the limit of large fetches can be evaluated by substituting F_{max} = 1.42 in (19) and (21) respectively. The results are, from (19), $(c_o/u_*)_{max}$ = 30.5, which is similar to the observational estimate of 34 [5], and from (21) $(\alpha_o)_{max}$ = 0.017 which is similar to the observational estimate of 0.019 [18].

4. The Inertial Coupling Relation

The observations reported in Sections 3.1 and 3.4, and in the main group of points in Section 3.2 are consistent with F ≈ 1, as was proposed in the original paper on inertial coupling [1]. The

observations are representative of oceanic and coastal environments. The data in Section 3.2 suggest that in more confined environments, F << 1, as indicated in Section 3.1.

The underlying physics which leads to these results is:

The two-dimensional turbulence of the atmosphere imposes a uniform spatial scale on the ocean, that can be interpreted as a 'moving' fetch, and hence a uniform, F, in which the kinetic energy is partitioned at the sea surface, such that in the absence of a surface shearing stress (τ_s) the kinetic energies of the atmospheric wind and the oceanic current would be expected to be equal. Thus, for $\tau_s = 0$, $\rho_1(u_1 - u_o)^2 = \rho_2(u_2 - u_o)^2$, which is satisfied by (5) with F = 1, which reduces to the inertial coupling relation,

$$u_* = {K_I}^{1/2}\left({\rho_1}^{1/2}(u_1 - u_o) - {\rho_2}^{1/2}(u_2 - u_o)\right)/{\rho_1}^{1/2} \tag{32}$$

On this basis we propose that the inertial coupling relation (32), which follows from the substitution of F = 1 in the similarity relations in the wave boundary layer, is of general applicability in large scale theoretical oceanic studies.

4.1 Reference Frames

The significance of two reference velocity (u_o) will now be considered.

4.1.1 The Surface Geostrophic Reference Frame

This is a very useful reference frame in which $u_o = u_{go}$ where u_{go} is the surface geostrophic velocity, which separates the frictional components from the geostrophic components. Here (32) may be expressed in the form,

$$u_* = {K_I}^{1/2}(u_{e1} - u_{e2}/\varepsilon) \tag{33}$$

where $u_{e1} = u_1 - u_{go}$ and $u_{e2} = u_2 - u_{go}$. The vector version of this reference frame ($\underline{u}_o = \underline{u}_{go}$), taking account of the horizontal variability of $\underline{u}_{go}$, has been used by the author in an ongoing research projects (An integrated theory of the air-sea boundary layer: Part I Surface friction on the large scale ocean circulation. *Unpublished ms.*).

The surface reference frame ($\underline{u}_o = \underline{u}_2$) could also be used, provided that the complex horizontal variability of $\underline{u}_2$ can be taken into account.

4.1.2 The Earth Reference Frame

This fundamental reference frame in which $\underline{u}_o = 0$ is of course used implicitly in most studies. The theoretical results of Section 2 use this reference frame although for completeness, u_o, is retained in the derivations.

5. Conclusions

The main conclusion is that it is possible to successfully predict the major properties of the wave boundary layer using a similarity representation for the air and the water velocity profiles. The model predicts the properties in terms of two parameters (F and R) which depend respectively on the fetch and duration of the wave environment, and importantly shows that F = 1, which was

assumed in the original inertial coupling relation for the air-sea boundary layer, is a good approximation for large scale ocean modelling studies. Hence, the important parameter is R, which increases in swell dominant environments (Section 3.4) and controls the input of energy from the wave field into the deep ocean. This process can be further examined in global eddy resolving ocean circulation modelling studies.

Author Contributions

The Author is solely responsible for this work.

Competing Interests

The author has declared no competing interests exists.

References

1. Bye JA. Inertial coupling of fluids with large density contrast. Phys lett A. 1995; 202: 222-224.
2. Greenslade D, Hemer M, Babanin A, Lowe R, Turner I, Power H, et al. 15 priorities for wind-waves research: An Australian perspective. Bull Am Meteorol Soc. 2020; 101: E446-E461.
3. Bye JA, Wolff JO. Momentum transfer at the ocean–atmosphere interface: The wave basis for the inertial coupling approach. Ocean Dyn. 2001; 52: 51-57.
4. Bye JA. The coupling of wave drift and wind velocity profiles. J Mar Res. 1988; 46: 457-472.
5. Toba Y. Local balance in the air-sea boundary processes: III. On the spectrum of wind waves. J Oceanogr. 1973; 29: 209-220.
6. Bye JA, Wolff JO. Charnock dynamics: A model for the velocity structure in the wave boundary layer of the air–sea interface. Ocean Dyn. 2008; 58: 31-42.
7. Bye JA, Wolff JO, Lettmann KA. A note on ocean surface drift with application to surface velocities measured with HF Radar. J Oceanogr. 2017; 73: 491-502.
8. Bye JA, Wolff JO, Lettmann KA. On the variability of the Charnock constant and the functional dependence of the drag coefficient on wind speed: Part II-Observations. Ocean Dyn. 2014; 64: 969-974.
9. Charnock H. Wind stress on a water surface. Q J R Meteorol Soc. 1955; 81: 639-640.
10. Bye JA, James C. Wave transport in the South Australian Basin. Cont Shelf Res. 2018; 154: 26-36.
11. Hasselmann K. Wave-driven inertial oscillations. Geophys Astrophys Fluid Dyn. 1970; 1: 463-502.
12. Babanin AV, Van der Weshuijsen A, Chalikov D, Rogers WE. Advanced wave modeling, including wave-current interaction. J Mar Res. 2017; 75: 239-262.
13. Wilson BW. Numerical prediction of ocean waves in the North Atlantic for December, 1959. Dtsch Hydrogr Zeitschrift. 1965; 18: 114-130.
14. Mitsuyasu H. Observations of the wind and waves in Hakata Bay. Rep Res Inst Appl Mech Kyushu Univ. 1971; 19: 37-74.
15. Bye JA, Ghantous M, Wolff JO. On the variability of the Charnock constant and the functional dependence of the drag coefficient on wind speed. Ocean Dyn. 2010; 60: 851-860.

16. Donelan MA, Dobson FW, Smith SD, Anderson RJ. On the dependence of sea surface roughness on wave development. J Phys Oceanogr. 1993; 23: 2143-2149.
17. Jones IS, Toba Y. Wind stress over the ocean. 2nd ed. Cambridge: Cambridge University Press; 2008. 307p.
18. Wu J. Wind-stress coefficients over sea surface near neutral conditions—A revisit. J Phys Oceanogr. 1980; 10: 727-740.